JACS
JOURNAL OF THE AMERICAN CHEMICAL SOCIETY
Article
pubs.acs.org/JACS

Energetics of Photoinduced Charge Migration within the Tryptophan Tetrad of an Animal (6–4) Photolyase

Fabien Cailliez,[†] Pavel Müller,[*,‡] Thiago Firmino,[†] Pascal Pernot,[†] and Aurélien de la Lande[*,†]

[†]Laboratoire de Chimie Physique, UMR 8000 CNRS/University Paris-Sud, University Paris-Saclay, 91405 Orsay, France
[‡]Institute for Integrative Biology of the Cell (I2BC), CEA, CNRS, University Paris-Sud, University Paris-Saclay, 91198 Gif-sur-Yvette cedex, France

Supporting Information

ABSTRACT: Cryptochromes and photolyases are flavoproteins that undergo cascades of electron/hole transfers after excitation of the flavin cofactor. It was recently discovered that animal (6–4) photolyases, as well as animal cryptochromes, feature a chain of four tryptophan residues, while other members of the family contain merely a tryptophan triad. Transient absorption spectroscopy measurements on *Xenopus laevis* (6–4) photolyase have shown that the fourth residue is effectively involved in photoreduction but at the same time could not unequivocally ascertain the final redox state of this residue. In this article, polarizable molecular dynamics simulations and constrained density functional theory calculations are carried out to reveal the energetics of charge migration along the tryptophan tetrad. Migration toward the fourth tryptophan is found to be thermodynamically favorable. Electron transfer mechanisms are sought either through an incoherent hopping mechanism or through a multiple sites tunneling process. The Jortner–Bixon formulation of electron transfer (ET) theory is employed to characterize the hopping mechanism. The interplay between electron transfer and relaxation of protein and solvent is analyzed in detail. Our simulations confirm that ET in (6–4) photolyase proceeds out of equilibrium. Multiple site tunneling is modeled with the recently proposed flickering resonance mechanism. Given the position of energy levels and the distribution of electronic coupling values, tunneling over three tryptophan residues may become competitive in some cases, although a hopping mechanism is likely to be the dominant channel. For both reactive channels, computed rates are very sensitive to the starting protein configuration, suggesting that both can take place and eventually be mixed, depending on the state of the system when photoexcitation takes place.

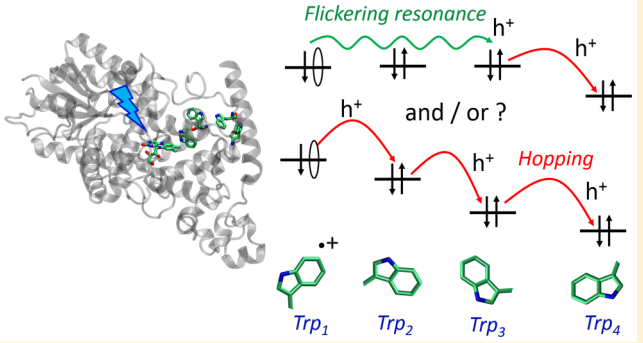

INTRODUCTION

Photolyases (PLs) and cryptochromes (CRYs) form a superfamily of flavoproteins that are found in all living organisms, ranging from bacteria and archaea to eukaryotes.[1−3]

PLs use the energy of blue to near-UV light to repair DNA damage induced by UV light. CRYs are responsible for various biological functions depending on the organisms in which they are expressed. In plants, they are blue-light receptors involved in photomorphogenesis, while in insects and mammals, they participate in the regulation of circadian rhythms, both as light receptors (animal type I cryptochromes) and as light-independent components within the complex circadian machinery.[3] Interestingly, CRYs are also suspected to be responsible for the ability of migratory species to perceive the Earth's magnetic field (through the so-called radical-pair mechanism).[4] Despite having versatile biological functions, PLs and CRYs share important structural elements: a highly conserved domain of ca. 400 amino acids harboring a noncovalently bound flavin adenine dinucleotide (FAD) cofactor. The vast majority of these proteins contain a triad of tryptophan residues, which can be involved in an ultrafast (subnanosecond) photoreduction of the flavin cofactor upon its electronic excitation. The dark redox state of FAD in CRYs and PLs in vivo is still a matter of debate, but isolated proteins tend to contain partially or fully oxidized flavin ($FADH^{\circ}/FAD_{ox}$). If this is the case also in vivo, photoreduction of FAD via the tryptophan chain provides a means to activate the proteins: conformational changes leading to light signaling by CRYs[5−7] are believed to be triggered by reduction of FAD_{ox} to the semiquinone ($FAD^{\circ-}/FADH^{\circ}$), and PLs need a fully reduced flavin $FADH^{-}$ in order to be active in DNA repair.[1]

Multiple in vivo studies (reviewed, for example in refs 8 and 9), the right (photo)chemistry of CRYs for a radical pair mechanism to be operational,[10] and the fact that they are present in the retina of birds and other animals[11] all point at the role of CRYs as the light-modulated sensors of the terrestrial magnetic field. The nature of the radical pair is however still under debate. A possible candidate is a $FAD^{\circ-}$ $Z^{\circ+}$ pair formed in CRYs upon the photoexcitation of FAD_{ox} and subsequent

Received: October 19, 2015
Published: January 14, 2016

DOI: 10.1021/jacs.5b10938
J. Am. Chem. Soc. 2016, 138, 1904−1915

charge migration along a tryptophan chain. Z could be a tryptophan radical,[4] but other proposals have been made.[12] An alternative to photoreduction is a $FADH^{\circ}/O_2^{\circ-}$ pair formed upon the dark reoxidation of a fully (photo)reduced flavin ($FADH^-$).[13−17]

The examples given above illustrate the need to understand the mechanisms of photoreduction in CRYs and PLs. The "tryptophan triad" has been a paradigm to account for flavin photoreduction in these proteins since the experiments of Brettel and collaborators on the *E. coli* cyclobutane pyrimidine dimer PL in 2000.[18] Recently, however, Müller et al. reported that several proteins of the cryptochrome/photolyase family contain a fourth tryptophan beyond the classical triad.[17] They examined photoreduction of the (6−4) photolyase from *Xenopus laevis* (the African clawed frog) by transient absorption spectroscopy in both wild-type protein and a mutant, in which Trp_{370} (the putative fourth redox-active tryptophan residue) was replaced by a nonreducing phenylalanine (Figure 1). The

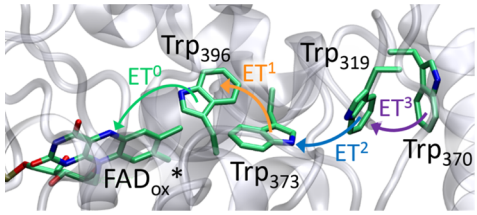

Figure 1. Charge migration within the Trp tetrad of *Xl*(6−4)PL after excitation of the oxidized FAD cofactor. Hydrogen atoms are omitted for clarity. Picture made with VMD.[46]

two proteins respond very differently to blue light excitation of FAD_{ox}. In particular, the wild-type system leads to a much longer-lived radical pair than the protein lacking the fourth Trp, therefore indicating different photoactivaton process and probably the formation of $Trp_{370}^{\circ+}$ in the wild-type PL. These findings shift the tryptophan triad paradigm to a tryptophan tetrad for animal (6−4)PLs and probably also for animal CRYs. Indeed, the fourth tryptophan is conserved in most if not all of these proteins. Possible implications for the photoactivation mechanism and for the magnetic compass ability of CRYs are discussed in ref 17. The results of Müller et al. clearly showed that the fourth Trp is involved in electron transfer to flavin. Nevertheless, it could not be unambiguously inferred from the data whether the fourth Trp really is the terminal electron donor or whether it only stabilizes the cation radical on the third tryptophan of the cascade.

Atomistically resolved numerical simulations have the potential to shed light on the intimate molecular mechanisms of the ultrafast electron transfers. In the past, various groups investigated photoinduced electron transfer events in PLs and CRYs.[19−24] Charge migration within tryptophan triads was investigated through molecular dynamics simulations and thermodynamics integration.[25] Elstner and co-workers used a density functional theory tight-binding-based (DFTB) molecular dynamics simulations approach to simulate ET within the tryptophan triad of *E. coli* PL and *Arabidopsis thaliana* CRY.[26−28] The present study is the first to address the specificities of charge migration within a Trp *tetrad* as the one contained in *Xl*(6−4) PL and the putatively magnetoreceptive animal cryptochromes. This article is therefore devoted to the investigation of the charge migration mechanism in *Xl*(6−4)PLs. Our numerical simulations combine polarizable molecular dynamics (MD) simulations with constrained density functional theory (cDFT).

An additional reason for studying electron transfers in PLs and CRYs comes from the time scale on which they occur. Indeed, besides charge migration in the photoreactive center (PRC), ETs in PLs and CRYs are the fastest known electron transfers in proteins. In the past, ETs have been customarily understood in the framework of Marcus theory (MT), which is an equilibrium theory.[29−31] However, for picosecond ETs as in PRC, PLs, and CRYs, it is clear that several nuclear vibrational modes are frozen on the time scale of electron transfer, making the applicability of Marcus theory questionable. It is therefore of particular interest to interrogate the interplay between such out-of-equilibrium nuclear motions and electron transfers which are potentially at the source of nonlinear or nonergodic effects. For instance, various groups investigated picosecond ET in the PRC that involve the special pair, the bacteriochlorophyll, and the bacteriopheophytin cofactors, arriving to the conclusion that the arrest of certain vibrational modes on ET time scale enables the systems to avoid large reorganization energies and leads to fast ET rates.[32−35] In the case of *E. coli* PL, Elstner and co-workers also observed noticeable deviation of ET rates predicted by the standard Marcus theory compared to the outcomes of direct DFTB-based nonadiabatic MD simulations of the ET process in the tryptophan triad.[25,26]

Finally, CRYs and PLs are extremely attractive natural model systems for studies of charge hopping involving amino-acid residues,[18] a phenomenon that is currently of growing interest.[35−42] It is yet to be established which reactive channels are at play in these phenomena. We take here the case of charge migration within the tryptophan tetrad of *Xl*(6−4)PL to address the competition between incoherent hopping and multiple sites coherent tunneling via the flickering resonance (FR) model recently proposed by Skourtis, Beratan, and co-workers.[43] The FR may provide a channel for electron transfers along the chain of redox cofactors having similar energies. Because of the novelty of this theoretical proposal, its applicability to real biological systems is still a matter of debate.[44,45]

This article is organized in three main sections. We first detail our computational protocol; then computational results are presented before being discussed and compared to the available experimental literature.

METHODS

Molecular Simulations of Electron Transfers. In this article we use molecular dynamics simulations to investigate charge migration in *Xl*(6−4)PL. Simulation protocols for studying electron transfer processes in proteins based on MD simulations are now rather well established.[30,47,48] Schematically, they can be classified into two categories: those that are based on the direct propagation in time of the electronic and nuclear degrees of freedom and those that rely on kinetic models. As a recent illustration of the first category, we mention the density functional theory tight binding-based approach of Elstner and co-workers.[49] Their methodology was applied to model charge migration in DNA,[50] DNA photolyases from *E. coli*,[26] and to a plant cryptochrome.[28] This type of approach is powerful in the sense that it does not presuppose any shape of the free energy surfaces, and it does not make any assumption regarding the relaxation time of the nuclear motion upon ET. The second category involves computation schemes that rely on kinetics models.[30,51] In the past, the mainstream approach was to simulate protein ET within the framework of the Marcus theory. The nonadiabatic rate can be calculated by the Fermi Golden Rule[29]

DOI: 10.1021/jacs.5b10938
J. Am. Chem. Soc. 2016, 138, 1904−1915

$$k_{ET} = \frac{2\pi}{\hbar}\langle H_{DA}{}^2\rangle \sum_{a,b} P(\varepsilon_a)|\langle\chi_a^i|\chi_b^f\rangle|^2\delta(E_i + \varepsilon_a - E_f - \varepsilon_b)a \quad (1)$$

where H_{DA} is the quantum mechanical coupling between the two electronic states. It can be obtained from quantum chemistry calculations or from semiempirical models.[48] $|\langle\chi_a^i|\chi_b^f\rangle|^2$ is the Franck−Condon (FC) factor between vibrational wave functions of the initial (i) and final (f) states, respectively. Indices a and b refer to two sets of vibrational levels associated with the vibrational modes. $P(\varepsilon_a)$ is the Boltzmann probability associated with the vibrational state a with energy ε_a. E_i and E_f are the electronic energies. The Dirac function ensures energy conservation. The active vibrational modes are those that make contributions to the FC factors. In this work we make a distinction between vibrations stemming from the tryptophan residues that are involved in ET (inner-sphere contributions) and vibrations of the environment (outer-sphere contributions: protein solvent, ...). The former are characterized by frequencies well above the thermal energy ($k_BT \approx 200$ cm^{-1} at 300 K) and must be treated quantum mechanically. On the other hand, the latter involve slower motions and can be taken into account by classical mechanics considerations. We thus adopt the following mixed quantum-classical rate expression[52−56]

$$k_{MT} = \frac{2\pi}{\hbar}\frac{1}{\sqrt{4\pi\lambda_o k_B T}}\langle H_{DA}{}^2\rangle \times \sum_{b\in Trp}|\langle\chi_0^i|\chi_b^f\rangle|^2 \exp\left(-\frac{(\Delta G^\circ + \Delta E_{vib} + \lambda_o)^2}{4\lambda_o k_B T}\right) \quad (2)$$

where ΔG^0 is the free energy of the reaction of the ET process and λ_o is the outer-sphere reorganization energy. $\Delta E_{vib} = \sum_{k=1}^{M} b_k\omega_k$ is the energy dissipated in the M vibrational modes of the tryptophan residues with frequencies ω_k and vibrational quantum levels b_k. To derive eq 2 we assumed that only the initial ground vibrational state ($|\chi_0^i\rangle$) is populated.

Warshel and co-workers showed how atomistic simulations could be connected to the MT through the linear response approximation (LRA).[30,57] If this approximation holds, parameters for the outer-sphere contributions can be extracted from the outputs of two MD simulations performed on the two electronic states involved in the ET

$$\Delta G^0 = \frac{1}{2}(\langle\Delta E\rangle_i + \langle\Delta E\rangle_f) \quad (3)$$

$$\lambda_o^{St} = \frac{1}{2}(\langle\Delta E\rangle_i - \langle\Delta E\rangle_f) \quad (4)$$

In these equations, $\langle\Delta E\rangle_x = \langle E_f - E_i\rangle_x$ denotes the mean interaction energy gap between the redox cofactors and their environment. ΔE is computed on a sample of structures obtained from a MD simulation on the electronic state x (x = i stands for the initial state, and x = f stands for the final state). The St superscript is used to emphasize that λ equals one-half the Stokes shift $\langle\Delta E\rangle_i - \langle\Delta E\rangle_f$.

Specific Issues for Ultrafast Electron Transfers. An alternative way to estimate the reorganization energy is from the variance of the energy gap, var (ΔE)[47]

$$\lambda_o^{var} = \frac{var(\Delta E)}{2k_BT} \quad (5)$$

If energy gap fluctuations follow Gaussian statistics (in which case the LRA applies) $\lambda_o^{St} = \lambda_o^{var}$. Matyushov and collaborators explored the validity and limitations of the LRA in the context of ultrafast (picosecond) intraproteic ET as encountered, for example, in charge separation within the PRC.[32,33,58] They reported large deviations between λ_o^{var} and λ_o^{St}. According to Matyushov et al., deviation from Gaussian statistics can arise due to nonergodicity of the system, i.e., electron transfer takes place on time scales on which some vibrational motions are frozen. Other sources of non-Gaussian statistics of energy gaps can be a large modification of protein structure upon electronic transfer or strong polarizability of the redox cofactors, like in the case of the special pair of the PRC.[59]

In this paper, we have chosen to compute the rates of electron transfer between successive tryptophans using the Jortner−Bixon formulation of Marcus theory with parameters computed with eqs 2−5. In order to address the problem of nonergodicity due to frozen vibration modes, we explored the influence of the sampling time used to compute the rates. Moreover, we probed the influence of the initial configuration. More details about the generation of these configurations are given later in the text.

Multistep Hopping vs Flickering Resonance. We consider two possible channels for charge migration within the tryptophan tetrad of *Xl*(6−4)PL. The first one is the multistep hopping (MH) mechanism by which one assumes a stepwise charge migration along the chain of cofactors. Electron/hole transfer between two adjacent tryptophans i and j takes place when electronic states $\{i^+,j\}$ and $\{i,j^+\}$ become quasi-degenerate or, more precisely, when the energy gap is smaller than the electronic coupling. Once the hole arrives on a tryptophan, the system is assumed to leave the region of quasi-degeneracy before the next ET can proceed. The individual rates for each step are calculated with eqs 2−4.

The second mechanism is based on the flickering resonance (FR) model recently put forward by Skourtis, Beratan, and co-workers.[43] The FR model has been devised to account for charge transfer along chains of redox cofactors. The model relies on the possibility to bring more than two electronic states at once into quasi-degeneracy. In such geometries, the electron is able to transfer ballistically (i.e., at constant speed) over more than two cofactors. The FR ET rate through an N-states system takes the form

$$k_{FR}(N) = \frac{1}{\tau} \times P_{match}(N) \quad (6)$$

where τ is the limiting characteristic time of the overall process and $P_{match}(N)$ is the probability that all electronic states differ by less than the electronic coupling H_{DA}[43]

$$P_{match}(N) = \int_{-\infty}^{-\infty} dH_{DA}\rho_H(H_{DA}) \int_{-\infty}^{-\infty} dE_1\rho_1(E_1) \times \int_{E_1-H_{DA}}^{E_1+H_{DA}} dE_2\rho_2(E_2)... \times \int_{\max\{E_1,...,E_{N-1}\}-H_{DA}}^{\min\{E_1,...,E_{N-1}\}+H_{DA}} dE_N\rho_N(E_N) \quad (7)$$

where $\rho_H(H_{DA})$ is the probability density function of the electronic coupling and $\rho_X(E_x)$ are the electron attachment/detachment density functions (site energies E_x). These are the energies used in Hopfield's theory of ET.[60] Analytical models based on independent oscillators have been derived in ref 43 to relate $P_{match}(N)$ to the Marcus theory parameters.[43] In order to be consistent with the mixed quantum-classical approach outlined above for the MT rate expression, we derived an analogous expression for P_{match} (assuming uncorrelated site energies)

$$P_{match}(N) = \int_{-\infty}^{-\infty} dH_{DA}\rho(H_{DA}) \times \int_{-\infty}^{-\infty} dE_1 \sum_{a_1} (FC)_{a_1}\rho^{o,a_1}(E_1) \times \int_{E_1-H_{DA}}^{E_1+H_{DA}} dE_2 \sum_{a_2} (FC)_{a_2}\rho^{o,a_2}(E_2) \times ... \int_{\max\{E_1,...,E_{N-1}\}-H_{DA}}^{\min\{E_1,...,E_{N-1}\}+H_{DA}} dE_N \sum_{a_N} (FC)_{a_N}\rho^{o,a_n}(E_N) \quad (8)$$

where $(FC)_{a_x}$ is the Franck−Condon factor of site x, characterized by the vibrational quantum numbers a_x. We assume that only the ground vibrational state of the Trp residue is populated in the initial electronic state. E_x is the outer-sphere contribution to the attachment/detachment energy function of site x. Its probability distribution (ρ^{o,a_x}) is centered at the average outer-sphere energy but shifted by the

DOI: 10.1021/jacs.5b10938
J. Am. Chem. Soc. 2016, 138, 1904−1915

energy associated with the vibrational levels a_x. Practical expressions are given in the next section. Equation 8 permits calculating the matching probabilities as a sum of branching channels over the inner-sphere vibrational levels.

Computational Protocol. The inner- and outer-sphere contributions to the ET rates have been calculated at the QM (quantum mechanics) and MM (molecular mechanics) levels, respectively.[47] The inner-sphere contribution enters via the FC factors $|\langle\chi_b^f|\chi_0^i\rangle|^2$ and the ΔE_{vib} energy terms (see eq 2). We used the molFC program[61] developed by Borrelli and Peluso to calculate these quantities from nuclear wave functions computed under the harmonic approximation.[62] Frequency calculations for the neutral and ionized species have been carried out at the DFT level with deMon2k[63] using the B3LYP functional and the 6-311G** basis set.[64,65] The GEN-A2* auxiliary basis set was used in the density fitting procedure. An important point is to determine k sets of relevant vibrational quantum numbers (vqn) $b_k = \{\nu_1, ..., \nu_m\}k$ (where ν_i refers to the vqn of the ith mode) to be included in the sum of FC factors (eq 2). This choice is guided by the displacements and the mixings of vibrational modes upon ET.[66,67] They have been computed based on the affine Duschinsky relationship[68] as implemented in molFC. For modes that are not displaced, ν_i was set to 0, while for displaced or mixed modes (the "active modes") ν_i was set to 0, 1, or 2 if $\omega_i < 1000$ cm^{-1} and to 0 or 1 if $\omega_i > 1000$ cm^{-1}. Note that it is not necessary to go beyond $\nu_i = 2$ because the nuclear overlaps with the initial ground vibrational become negligible and because since ET between Trp residues takes place in the normal region (see Result section), the ΔE_{vib} terms become too large to contribute significantly to ET rates. For the calculations of the ET rates, only FC factors that are larger than 10^{-8} were retained.

The outer-sphere contributions are obtained through eqs 3 and 4, restricting the contributions to the energy gap to interactions between the tryptophans and the environment and between the tryptophans involved in ET

$$\Delta E^0 = [E_f^{MM} - E_f^{MM}(D) - E_f^{MM}(A^+)] - [E_i^{MM} - E_i^{MM}(D^+) - E_i^{MM}(A)] \quad (9)$$

where E_x^{MM} is the energy of the whole system computed with the force field describing electronic state x and $E_x^{MM}(X)$ is the internal energy contribution due to the donor (X = D) or the acceptor (X = A) moiety in this same electronic state. ΔE^0 captures the electrostatic contributions between permanent charges, between permanent charges and induced dipoles, and between induced dipoles. Induced dipoles are calculated self-consistently from the electric field created by permanent charges and by other induced dipoles.

A QM+MM strategy has been applied for calculating the FR matching probabilities. The probability function for the oxidation of an electron donor along the chain is assumed to be Gaussian (the assumption turned out to be justified)

$$\rho_{D/D+}^{o,a_x}(\Delta E_D^{ox}) = \frac{1}{\sqrt{2\pi}\sigma_D}\exp\left(\frac{-(\Delta E_D^{ox} - \overline{\Delta E_D^{ox}})^2}{2\sigma_D^2}\right) \quad (10)$$

with

$$\Delta E_D^{ox} = E_{D+} - E_D = [E_{D+}^{MM} - E_{D+}^{MM}(D^+)] - [E_D^{MM} - E_D^{MM}(D)] \quad (11)$$

The center of the Gaussian distribution is given by $\overline{\Delta E_D^{ox}}$ which is defined as the sum of the mean ΔE_D^{ox} value and the inner-sphere term $\Delta E_{D/D+}^{inner} = \Delta E_{D/D+}^{i} + \sum_{k=1}^{M} a_{x,k}\omega_k$. In this latter expression the first term on the right-hand side is the difference between the bottoms of the potential wells of the oxidized and reduced forms of the Trp residue (including zero-point energy corrections) while the second term is the vibrational energy of site x associated with the set of vqn $a_{x,k}$. The Gaussian widths σ_D are computed from the variance of energy gaps formula (eq 5) according to

$$\sigma_D = \sqrt{2k_BT\lambda_o^{var}} \quad (12)$$

Similarly, the probability function for the reduction of an electron acceptor reads

$$\rho_{A+/A}^{o,a_x}(\Delta E_{A+}^{red}) = \frac{1}{\sqrt{2\pi}\sigma_{A+}}\exp\left(\frac{-(\Delta E_{A+}^{red} - \overline{\Delta E_{A+}^{red}})^2}{2\sigma_{A+}^2}\right) \quad (13)$$

with

$$\Delta E_{A+/A}^{red} = E_A - E_{A+} = [E_A^{MM} - E_A^{MM}(A)] - [E_{A+}^{MM} - E_{A+}^{MM}(A^+)] \quad (14)$$

The matching probability for shifting the hole on the initial oxidized tryptophan residue to the Nth tryptophan is obtained by numerically integrating eq 8 with the probability distributions of the site energies given by eqs 10–14.[43] The characteristic time τ appearing in eq 6 has been calculated in the following way. For $N = 2$, the MT and the FR are expected to lead to similar rate estimates and, in the hypothesis of constant electronic coupling τ, can be related to the Rabi time: $\tau = \tau_{Rabi}/\pi^2 = \hbar/\pi H_{DA}$. For $N > 2$, τ was calculated like in ref 43 from an estimate of the mean velocity of the transferred electron along the chain of redox cofactors. $\tau \approx R_{DA}\hbar/2r_{nn}H_{DA,nn}$, with r_{nn} and $H_{DA,nn}$ being the distance and electronic coupling for the closest pair of cofactors (see Table 1). This expression is certainly a crude approximation to the true dynamics of the tunneling electron, but in the absence of a more satisfying model it has been used in the present study.

Table 1. Average Unsigned Electronic Coupling and Inter-Tryptophan Position Descriptors[a]

	$Trp_{373} \rightarrow Trp_{396}^{o+}$	$Trp_{319} \rightarrow Trp_{373}^{o+}$	$Trp_{370} \rightarrow Trp_{319}^{o+}$
MD on initial state			
$\lvert H_{DA}\rvert$(meV)	27 (15)	23 (14)	38 (26)
d_{ij} (Trp_i–Trp_j) (Å)[b]	3.79 (0.21)	3.94 (0.31)	3.51 (0.20)
θ_{ij} (Trp_i–Trp_j) (deg)	28 (7)	82 (10)	41 (9)
φ_{ij} (Trp_i–Trp_j) (deg)[c]	50 (3)	34 (5)	104 (3)
γ_{ij} (Trp_i–Trp_j) (deg)	158 (6)	41 (9)	20 (11)
MD on final state			
$\lvert H_{DA}\rvert$ (meV)	24 (15)	29 (13)	37 (27)
d_{ij} (Trp_i–Trp_j) (Å)[b]	3.87 (0.21)	4.04 (0.32)	3.49 (0.21)
θ_{ij} (Trp_i–Trp_j) (deg)	29 (6)	85 (8)	37 (10)
φ_{ij} (Trp_i–Trp_j) (deg)[c]	50 (3)	36 (6)	103 (4)
γ_{ij} (Trp_i–Trp_j) (deg)	161 (7)	36 (9)	23 (14)

[a]Numbers in brackets are the standard deviations. The statistical uncertainties on $|H_{DA}|$ have been calculated by a block average technique for a 95% confidence interval. They amount to 3 meV in all cases. [b]Edge-to-edge distance between tryptophan side chains restricted to heavy atoms. [c]Average between φ'_{ij} and φ_{ij}, see Scheme 2.

The advantage of the QM+MM scheme over brute force QM/MM MD simulations (e.g., DFT/MM) is that we can afford MD simulations on the nanosecond time scale required to address the question of the interplay between nuclear relaxation times and electron transfer. DFT/MM MD would be much more CPU time consuming, and such simulations would likely be restricted to the picosecond time scale. An alternative would be to perform single-point DFT/MM calculations on top of classical MD simulations. However, such a strategy would require a tight calibration of the force field (intra- and intermolecular energy terms) to match as closely as possible the DFT/MM potential energy function. Experiences reported by other groups, for example, on iron or copper proteins, indicate that QM/MM approaches do not guarantee better results than purely MM when evaluating the outer-sphere contributions to redox processes.[47,69] It seemed therefore preferable to rely on the already calibrated AMBER ff02 force field[70] that additionally has the advantage to take account of induction. Previous works validated the use of the AMBER ff02 and the POL3 polarizable water model[70,71] to calculate outer-sphere

DOI: 10.1021/jacs.5b10938
J. Am. Chem. Soc. 2016, 138, 1904–1915

reorganization energies of redox processes.[72,73] We validated the QM+MM approach by comparison with short DFT/MM MD simulations (see SI).

Details of MD Simulations. All MD simulations were carried out with Amber 10[74] using the polarizable ff02 force field for proteins and nucleic acids and the polarizable POL3 model for water. Force field parameters of the riboflavin moiety of the FAD cofactor in the oxidized and in the semiquinone forms were taken from our previous study of ET in *Arabidopsis thaliana* cryptochrome.[22] To make the QM+MM scheme applicable, the side chains of tryptophans 396, 373, 319, and 370 were made nonpolarizable. Since no crystal structure of *Xenopus laevis* (6–4) photolyase has been reported so far, our initial structure was obtained by homology modeling using the SWISS-MODEL platform.[75] The best fit between the known sequence of *Xl*(6–4)PL[76] and that of a protein with a known crystal structure was obtained for the *Drosophila melanogaster* (6–4)PL (58% of the amino acid residues are identical and another 21% are chemically similar in the two proteins). The sequence of *Xl*(6–4)PL was aligned to the known structure of *Dm*(6–4)PL.[77]

Protonation states of amino-acid residues were determined based on pK_a estimates obtained from the PROPKA server.[78] After addition of hydrogen atoms, the system was solvated in a water box of dimensions 114 × 108 × 100 Å^3. Positions of hydrogen atoms were first geometrically optimized keeping heavy atoms fixed. Subsequently, water molecules and the full system were optimized in a total of 10 000 optimization steps. MD simulation was launched from this optimized structure. We used a time step of 1 fs to propagate the Newton equations of motion. Nonbonded interactions were evaluated with the particle mesh Ewald method using a grid spacing of 1 Å and a cutoff of 10 Å for calculating the direct space summation of electrostatic interactions. Induced dipoles were optimized with a tolerance of 10^{-6} Debye on the optimized structure and subsequently propagated along MD simulations through the Car–Parrinello scheme implemented in Amber 10 with default parameters. Thermal equilibration of the *Xl*(6–4)PL in the ground state was achieved by first running a 500 ps NVT simulation with strong harmonic restraints (50 kcal/mol/Å^2) on protein atoms positions. This was followed by five successive 200 ps MD trajectories in the NPT ensemble during which the harmonic restraints were gradually decreased: 50, 20, 10, 5, and finally 1 kcal/mol/Å^2. The system was finally relaxed for 8.6 ns without any constraint. Trajectories were then continued for 9.4 ns on the ground state to provide the starting conditions of MD simulations of the charge transfer states, as detailed below. The RMSD of the protein backbone atoms shown in Figure S1 indicate that no important structural change took place, attesting to the stability of the model.

The protocol followed in this study is aimed to address the issues of nonergodicity and nonequilibrium, due to the high ET rate in *Xl*(6–4)PL. Although inspired by the work of Matyushov and collaborators on electron transfers in the PRC[32,33] we did not follow the same methodology. We will come back to the comparison between the two approaches in the Discussion section. Our computational protocol is comprised of 26 sets of 4 × 500 ps MD simulations (Scheme 1). In the following, the notations CT1, CT2, CT3, and CT4 will stand for electronic states corresponding to the +1 charge localized on Trp 396, 373, 319, and 370, respectively. Each set begins with an MD simulation launched for 500 ps on the CT1 potential energy surface with initial conditions (nuclear positions and velocities) sampled from the resting state MD simulation. Note that we make the reasonable hypothesis that since the primary ET step from Trp396 to FAD* (producing FAD°$^-$,Trp396°$^+$, i.e., state CT1) is ultrafast (<1 ps), the geometries sampled from the ground state are suitable to launch MD simulations on state CT1. A MD trajectory on the CT2 potential energy surface is launched after 25 ps. A 25 ps delay is motivated by the characteristic time of the ET steps that were all found in the 1–100 ps time scale (see Results section). It would therefore not be justified to let the system relax for longer times on state CT1 before launching trajectories on CT2 state.[51] Similarly, MD trajectories on CT3 are launched after 25 ps of MD simulation on CT2, and so forth for the fourth charge transfer state. Dependence of the ET parameters to the simulation length will be analyzed in the Results section. The

Scheme 1. Simulation Protocol Used in This Study To Investigate Charge Migration within the Tryptophan Tetrad of *Xl*(6-4)PL[a]

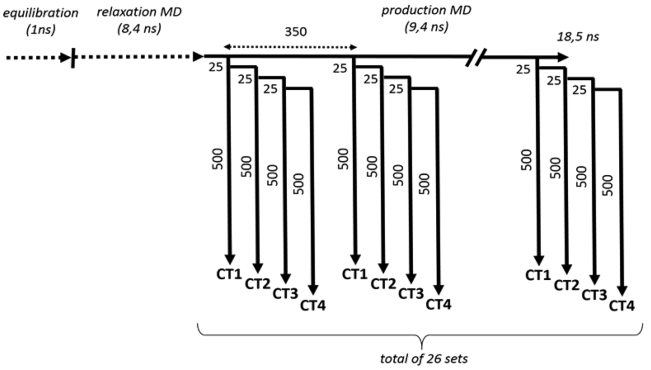

[a]The horizontal and vertical arrows represent MD simulations performed on the ground (resting) state and on the charge transfer states, respectively. Unless otherwise stated the numbers are given in picoseconds.

initial positions and velocities for starting trajectories on CT1 state were sampled every 350 ps from the MD simulations on the ground state, ensuring a minimal correlation between sets. Snapshots were extracted every 0.1 ps to calculate the vertical energy gaps.

Electronic Coupling Calculations. Electronic coupling values (H_{DA}) between charge transfer states were calculated from snapshots extracted every 10 ps along all the MD trajectories of CT1–CT4. For each ET step, we accumulated a total of 2600 evaluations using constrained density functional theory (cDFT) calculations.[79] To calculate the ET rates H_{DA} should in principle be sampled from geometries of quasi-degeneracy of the diabatic ET states. We will nevertheless make the assumption that the distribution of H_{DA} calculated without this energy restriction condition is adequate to calculate the rates. Details of cDFT implementation in deMon2k can be found elsewhere,[80,81] and we only mention here the most important calculation parameters. For a given ET step, the two side chains of the involved tryptophan residues were treated at the DFT level, while the remaining atoms were included as point charges in the Kohn–Sham Hamiltonian. One hydrogen atom was added to each methyl-indole group to saturate the valence of carbon atoms. We used the DZVP-GGA basis set (double zeta with valence polarization functions calibrated for generalized gradient approximation functionals)[82] in combination with the automatically generated GEN-A2/GEN-A2* auxiliary basis sets. Following recent benchmarks[83,84] we chose the hybrid PBE functional[85] with 50% of GGA exchange replaced by Hartree–Fock exchange. The contributions of Fock exchange to the Kohn–Sham potential were calculated by the variational fitting approach described in ref 86. To access the two diabatic states by cDFT we imposed the net charge difference between the electron donor and the electron acceptor to be equal to 1 or −1. Atomic charges were defined according to the standard Hirshfeld scheme.[87] Once Kohn–Sham determinants for the two diabatic states of interest were obtained, H_{DA} was calculated with the projection method described in ref 88.

Data Analysis and Uncertainty Calculations. Data analyses have been carried out with the R environment for statistical computing.[89] We used the CODA package to estimate the statistical chain inefficiencies generated by the MD simulations.[90] Details of the uncertainties calculation for each quantity discussed in this article can be found in the SI.

RESULTS

The aim of the present study is to decipher the mechanisms of photoinduced charge migration within the tryptophan tetrad of *Xl*(6–4)PL. By analogy with other proteins of the PL and CRY

DOI: 10.1021/jacs.5b10938
J. Am. Chem. Soc. 2016, 138, 1904–1915

superfamily which contain a fully oxidized FAD cofactor in the resting state, the primary ET step from Trp_{396} to FAD*, denoted ET^0 in Figure 1, is expected to take place on a subpicosecond time scale.[91−94] We will not consider this ultrafast primary process here and investigate instead the slower electron transfer steps ET^1, ET^2, and ET^3 along the tryptophan chain. We first present results concerning the driving forces, reorganization energies, and mean electronic couplings. We then compare the multistep hopping model based on Marcus theory and the flickering resonance model for estimating ET rates in this protein.

Effective Free Energy of Reaction and Outer-Sphere Reorganization Energies. For the sake of clarity, we start by focusing on the first electron transfer step $Trp_{373} \rightarrow Trp_{396}^{o+}$. As explained in the Introduction, it is likely that several nuclear motions do not have time to relax upon ET and are frozen on the ET time scale. Therefore, a first interrogation is the sensitivity of the effective free energy of reaction (Δg_o) and reorganization energies (λ_o^{St}), calculated by eqs 3 and 4, to the sampling length. The term "effective" is used here to emphasize that Δg_o departs from a genuine free energy function since it is computed from a limited ensemble of configurations that do not span the entire phase space accessible to the system at the considered temperature (here 300 K). Figure 2 thus depicts the evolution of Δg_o and λ_o^{St} as a function of the accumulated simulation length for each of the 26 sets of MD simulations. The 26 pairs of trajectories differ by the initial conditions of the simulation (nuclear positions and momenta, see the Methods section). For each of them we observe significant variations when increasing the length of the trajectories. For a given pair of trajectories these variations can be up to 0.2 eV for sampling lengths less than 100 ps. Fluctuations of Δg_o and λ_o^{St} are caused by nuclear vibrations that do not equilibrate on the 1−100 ps time scale. For simulation lengths greater than 250 ps, sharp fluctuations vanish but the values of both quantities clearly do not reach plateaus in all trajectories. Reorganization energies λ_o^{var} calculated from the variance of the energy gap (eq 5) are also highly dependent on the accumulated simulation time and on the initial conditions (Figure S2). Some of the curves can exhibit sharp variations and increase up to 1 eV. Finally, none of the Δg_o, λ_o^{St}, or λ_o^{var} quantities converges to common values after 500 ps. At this time, these parameters are scattered over a few tenths of electronvolts.

Despite these differences between each pair of trajectories, common features can be identified. For example, Δg_o is always predicted to be negative. Importantly, averaging over the 26 sets almost completely smooths out the fluctuations seen on the individual trajectories for each quantity of interest. The average curves vary within only a few hundredths of electronvolts in the first 100 ps. These results indicate that averaging over multiple starting conditions enables the determination of effective mean driving forces ($-\Delta g_o$) and reorganization energies that are numerically stable on the 1−500 ps time scale.

The analysis for the first electron transfer is also applicable for the $Trp_{319} \rightarrow Trp_{373}^{o+}$ and $Trp_{370} \rightarrow Trp_{319}^{o+}$ electron transfer steps, as can be seen from the graphs shown in Figures S3 and S4.

Figure 3 compares the average values of Δg_o and λ_o^{St} for the three electron transfer steps as a function of simulation length. $\overline{\Delta g_o}$ is negative for the three ETs, showing the downhill character of charge migration along the *Xl*(6−4) photolyase

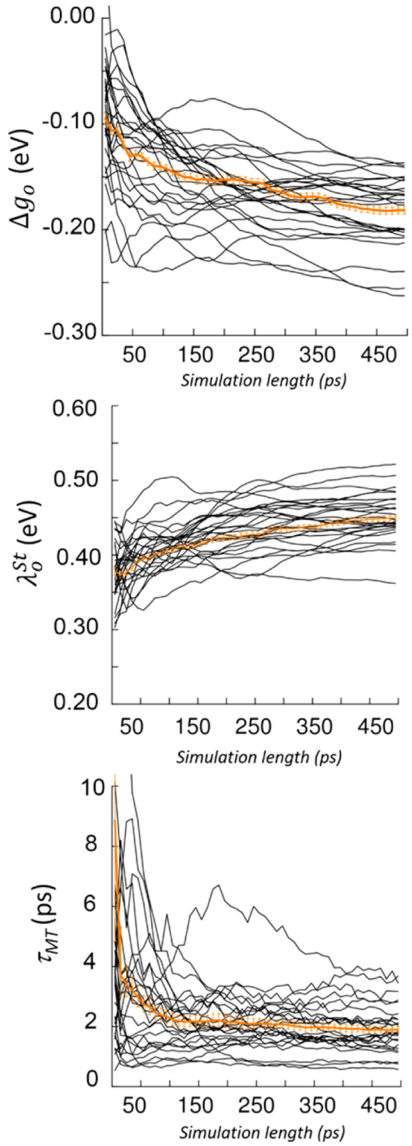

Figure 2. Electron transfer parameters and characteristic time as a function of accumulated simulation time for ET^1. Black and orange curves correspond to each of the 26 repetitions and to the average curve, respectively. For clarity, we depict error bars only for the average curve. Those of the individual curves are approximately 5 ($\approx\sqrt{26}$) times larger (see text and SI for details).

tryptophan tetrad. The first and third steps are characterized by a relatively modest value of $\overline{\Delta g_o}$, around −0.15 eV. The second electron transfer, on the other hand, is significantly more exergonic (−0.32 eV). The outer-sphere reorganization energy increases from 0.4 eV for the first step to almost 0.8 eV for the second step and finally decreases slightly for the final step (0.60−0.65 eV).

To better understand this trend we decomposed $\overline{\lambda_o^{St}}$ into contributions originating from the different parts of the molecular system, namely, the protein residues, the FAD cofactor, and the solvent (water and counterions). This analysis is made for a simulation length of 100 ps (similar decomposition is obtained for different simulation lengths). We stress that because of the use of a nonadditive polarizable force field in this study, the outer-sphere energy gap ΔE that is used to calculate $\overline{\lambda_o^{St}}$ cannot be unambiguously decomposed as

DOI: 10.1021/jacs.5b10938
J. Am. Chem. Soc. 2016, 138, 1904−1915

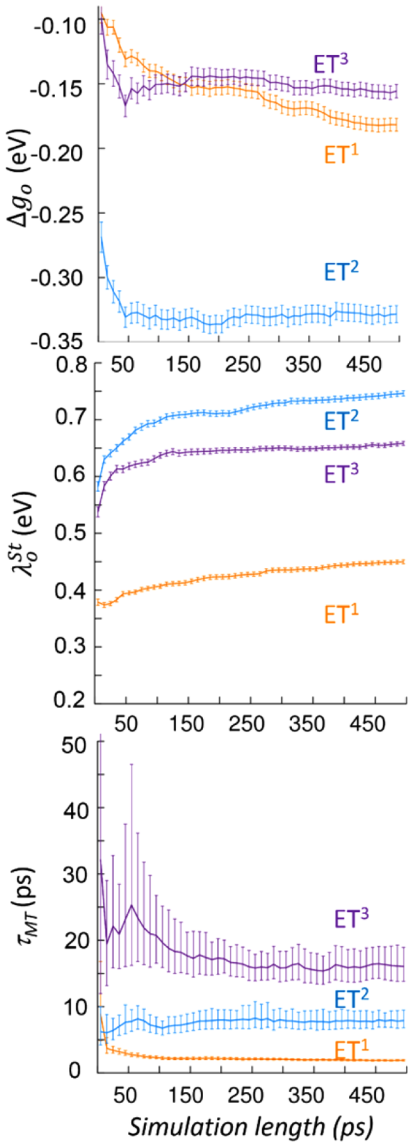

Figure 3. Time dependence of electron transfer parameters ($\overline{\Delta g_o}$ and $\overline{\lambda_o}$) and characteristic time (τ_{MT}) as a function of simulation length. Averages are performed over sets of 26 MD simulations. Error bars reflect the statistical uncertainties for a confidence interval of 95%.

a sum of contributions arising from different groups of atoms. This limitation is not purely methodological but actually correctly reflects the nonadditive nature of electrostatic induction. To circumvent this difficulty, we based our analysis on the permanent charge−charge Coulomb interaction between atoms, which is additive (i.e., $\Delta E_{coul} = \Delta E_{coul}^{protein-FAD} + \Delta E_{coul}^{water}$). The total Coulomb interaction ΔE_{coul} correlates reasonably well with the total energy gap ΔE that captures induction contributions. The linear regression parameter R^2 between the two quantities was found in the 0.8−0.9 range. Each Coulomb contribution was thus multiplied by the slope of a linear regression, leading to corrected Coulomb contributions ΔE_X^{corr}, from which reorganization energies λ_X^{St} were calculated. The sum of ΔE_X^{corr} (respectively λ_X^{St}) almost equals ΔE (respectively, λ^{St}), the remaining difference being expressed as a residual contribution (that represents 10−20%).

As can be seen from the histograms plotted in Figure 4, the rise of ∼0.4 eV from the first to the second ET step comes partly from the increased contribution of the protein (0.18 eV) and, to a lesser extent, from water (0.09 eV). The decrease in reorganization energy in the third ET step results from a smaller contribution from the protein, counterbalanced by a larger contribution from water.

As charge migration progresses along the tryptophan tetrad the contribution of solvent to the reorganization energy increases. This trend is to be related to the degrees of solvation of the tryptophan residues as seen from the radial distribution functions depicted in Figure 4. While Trp_{396} and Trp_{373} are protected from the solvent, Trp_{319} and Trp_{370} are clearly more exposed. A similar graph has been reported by Lüdemann et al.[28] for the tryptophan triad of *E. coli* photolyase. These authors remarked that the second tryptophan was desolvated, in contrast to that of *Arabidopsis thaliana* cryptochrome that is largely exposed to the solvent.[28] Our simulations of *Xl*(6−4) photolyase reveal that the second tryptophan is, like in *E. coli* photolyase, largely unsolvated. Actually, analysis of available crystallographic structures of animal cryptochromes (which possess a tryptophan tetrad like the (6−4) photolyase) also points to an unsolvated second tryptophan, maybe due to the presence of a methionine residue in its vicinity (Met_{308} in *Xl*(6−4) PL numbering). Future MD simulations on various members of the PLs and CRYs superfamily would be needed to systematically assess the influence of tryptophan solvation degree on the charge migration process.

Electronic Coupling. The strength of the coupling between electronic states involved in charge migration is a

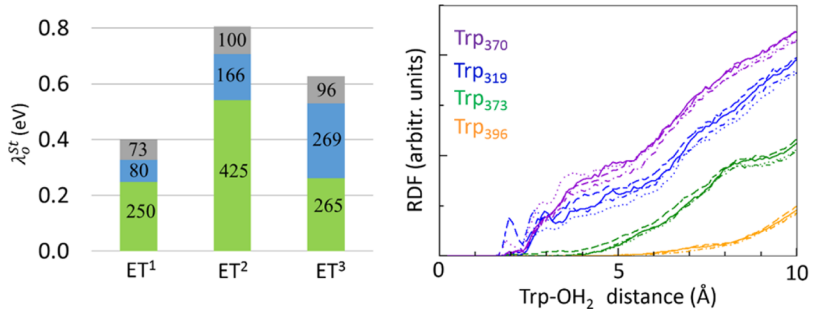

Figure 4. (Left) Contributions to the reorganization energy of the system constituents for the three electron transfer steps along the Trp tetrad: protein and FAD (green), water and counterions (blue), and residual contributions (gray, see main text). Contributions given inside the bars are given in meV. (Right) Radial distribution of water around the four tryptophan moieties from MD simulations performed on CT1 (full lines), CT2 (dashed lines), CT3 (dash-dotted lines), and CT4 (dotted lines) states.

DOI: 10.1021/jacs.5b10938
J. Am. Chem. Soc. 2016, 138, 1904−1915

Scheme 2. Geometrical Parameters Characterizing the Relative Positions of a Pair or Tryptophan Side Chains in *Xl*(6-4)PL

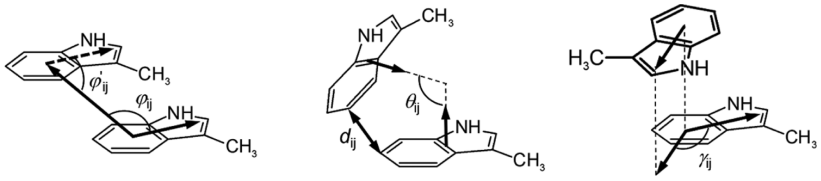

key parameter governing electron transfer processes. We computed H_{DA} at the constrained DFT level over 2600 configurations for each of the three ET steps (Table 1). $|H_{DA}|$ falls in a range of a few hundredths of electronvolts with standard deviations of the same order. The variation of average edge-to-edge distance d_{ij} between the tryptophan side chains grossly accounts for the variations of $|H_{DA}|$: the first two ET steps exhibit rather similar $|H_{DA}|$, while the third ET step is characterized by a higher $|H_{DA}|$ in line with the variations of intersite distances. More subtle fluctuations of the electronic coupling like those observed for a given pair of tryptophans along the MD simulations are difficult to rationalize.

H_{DA} between tryptophan residues is related to the overlap between the donor/acceptor π/π^* molecular orbitals that are localized on the indole rings. H_{DA} is thus expected to depend not only on d_{ij} but also on the relative angular orientation between them (Scheme 2). The relative orientation is quantified here by three angles: θ_{ij} is the angle between the normal vectors of the planes formed by the indole rings, φ_{ij} characterizes the relative sliding of the two planes, and finally γ_{ij} represents the relative rotation of the two rings. Average and standard deviations of these parameters are given in Table 1. We could not find simple relationships between $|H_{DA}|$ and any of these geometrical parameters (Figure S5). Electronic coupling fluctuations in photolyase are thus apparently multifactorial and span a range of several millielectronvolts.

We finally note that we found no significant variations of $|H_{DA}|$ before and after electron transfer. This is consistent with the fact that the relative positions of the tryptophan residues do not vary on the time scale of our MD simulations (500 ps), as seen from the averages of the geometrical parameters defined above. For each ET step an average value $|H_{DA}|^2$ will be used to calculate the rates.

Electron Transfer Rates. We estimated the electron transfer rates k_{ET} using either a multistate hopping model based on the Marcus parameters (eq 1) or via the flickering resonance mechanism (eq 7). For the hopping model, the average characteristic ET times ($k_{MT}^{-1} \equiv \tau_{MT}$) are on the order of a few picoseconds to a few tens of pisoseconds (Figure 3). For the three steps, τ_{MT} is sensitive to the simulation length and to the initial conditions, as a consequence of the sensitivity of the MT parameters as described above (Figures 1 S3 and S4).

For simulation lengths shorter than 20 ps, both the first and the second steps take place at similar rates given the statistical uncertainties associated with the estimation of τ_{MT} (5−20 ps). The third ET step is significantly slower (20−30 ps), in agreement with lower $\overline{\Delta g_o}$ combined with higher $\overline{\lambda_o^{St}}$. The analysis of the inner-sphere contribution to the rates is reported in Table 2. We will restrict our discussion to the second ET step (similar values were found for the first and third steps). Only contributions to the sum over the FC factors in eq 2 that are larger than 1% are reported in the table. Displacements of the normal modes upon oxidation/reduction of the tryptophan and of the tryptophanyl radical, respectively, are shown in Figure S6. The leading term is the one involving the overlap between the initial and the final ground vibrational states (71%). The only significant secondary contributions involve the first vibrational excited states of two modes at 600 and 617 cm^{-1} of the Trp^+ and Trp moieties, respectively. The displacement of these modes is close to 0.66. They correspond to nonsymmetric in-plane deformations of the indole ring. ET toward vibrationally excited states of most of the mixed or displaced modes, though numerous (see Figure S6), have a negligible contribution to the rates. This is in fact not surprising since the ET steps described in this work take place in the normal region of the Marcus theory.

Table 2. Inner-Sphere Contributions to the ET Rates

	FC[a]	ΔE_{vib} (cm^{-1})	vib state[b]	Ccontribution (%)[c]
1	0.0979	0	$\langle 0\|0\rangle$	71
2	0.0213	600	$\langle 0\|0.\ \nu^1_{Trp^+-8}\rangle$	6
3	0.0206	617	$\langle 0\|0.\ \nu^1_{Trp-9}\rangle$	6
4	0.0906	1548	$\langle 0\|0.\ \nu^1_{Trp-33}\rangle$	2
5	0.0318	1142	$\langle 0\|0.\ \nu^1_{Trp-23}\rangle$	1
6	0.0516	1481	$\langle 0\|0.\ \nu^1_{Trp^+-31}\rangle$	1

[a]Square of the vibrational overlap. [b]$\langle 0|0\rangle$ denotes the overlap between the vibrational ground states in the initial and final electronic states. The notation $|\nu^x_{Y-M}\rangle$ refers a vibrational state obtained by exciting the Mth normal mode of tryptophan Y in its xth excitation level, the remaining modes kept in the zeroth level. [c]Contribution of this pair of vibrational states to the overall ET rate calculated by eq 2.

Table 3. Flickering Resonance Model and Charge Migration in *Xl*(6-4)PL

N	2	3	4
$\overline{\Delta E_D^{ox}}$ (eV)[a]	0.27 (0.04)	0.33 (0.11)	0.33 (0.09)
σ_D (eV)	0.18 (<0.01)	0.20 (<0.01)	0.21 (<0.01)
$1/\tau$ (ps^{-1})	128.9	40.2	36.1
P_{match} (N)	5.75×10^{-3} (1.23×10^{-3})	1.23×10^{-4} (5.64×10^{-5})	3.11×10^{-6} (1.83×10^{-6})
τ_{FR} (ps)	1.45 (6.81)	202 (440)	8907 (15 146)

[a]Values corresponding to the FR channel between the ground vibrational level, additional shifts appear when excited vibrational states are involved (see Methods section). An offset of $-\overline{\Delta E_{A+}^{red}}$ has been applied, setting the average site energy of the initial oxidized $Trp_{396}{}^{o+}$ to zero. We report averages over 26 sets of MD trajectories with standard deviations given in brackets.

We now turn to the FR model. Table 3 gathers the parameters of the site energy probability distributions ($\overline{\Delta E_D^{ox}}$, σ_D, eq 10), the matching probabilities, and the characteristic ET times ($k_{FR}{}^{-1} \equiv \tau_{FR}$) predicted by the FR model. We assumed the FR channel to be limited by the electron transport time (τ_{trans}) through the Trp chain when resonance is established ($\tau \approx \tau_{trans}$, see eq 6). We set the system in the CT1 state

DOI: 10.1021/jacs.5b10938
J. Am. Chem. Soc. 2016, 138, 1904−1915

(Trp_{396}^{o+}) and estimate the time to shift the +1 charge to Trp_{373} (N = 2 sites), Trp_{319} (N = 3), or Trp_{370} (N = 4). The electronic coupling is for now set to its average value (0.025 eV). In principle, the matching probabilities could be sensitive to the accumulated simulation times as for the Marcus theory parameters. It turns out, however, that this is the case only to a small extent. We thus base our discussion on the data obtained with an accumulation time of 100 ps. By contrast, the matching probabilities are very sensitive to the initial conditions as can be seen from the standard deviations given in Table 3.

For N = 2, τ_{FR} closely matches τ_{MT} (1.45 vs. 2.0 ps). This is expected since both models can be shown to be identical in the nonadiabatic regime with constant electronic coupling.[43] This correspondence is also true with the mixed quantum-classical formalism used in this work (eq 2 and eq 8).

For N = 3, the average time over the 26 sets of MD simulations is 202 ps with a standard deviation as large as 440 ps. For some of the MD simulations, τ_{FR} has a value of a few picoseconds. Finally, for N = 4, ET is expected to take place on the nanosecond time scale.

Setting as a reference the energy of the acceptor site (Trp_{396}^{o+}) to 0.0, the bridge sites lie ca. 0.33 eV higher within an energy window of less than 0.1 eV. The widths of the site energy distributions are 0.20 eV, which is only slightly less than the difference between mean site energies. Little dispersion of the widths due to the starting conditions is observed. On the other hand, the mean site energies are far more sensitive to the starting conditions (e.g., 0.11 for N = 3). Consequently, in rare cases of closest energy proximity of the mean site energies, large overlaps of the site energy distributions can be obtained and hence significant matching probabilities. Recall that an electronic coupling of a few hundredths of electronvolts has been used to compute the matching probabilities of Table 3. Under the hypothesis that the transport time is limiting, the FR channel for N = 3 can be competitive for a few sets of initial configurations.

Besides the sensitivity to the initial conditions, it is worth remarking that FR rates are highly sensitive to the electronic coupling H_{DA} used to integrate the matching probabilities and the transport time τ. τ_{FR} can vary by several orders of magnitude when scanning the continuum of H_{DA} values sampled during MD simulations. For the smallest coupling values (0.005 eV), the matching probability drops dramatically because the energy windows of allowed electronic population exchanges become narrower, i.e., the degeneracy condition ($\Delta E_{ij} < H_{DA}$) becomes extremely tight. Figure 5 also illustrates the sensitivity of τ_{FR} with the initial conditions for different values of H_{DA}.

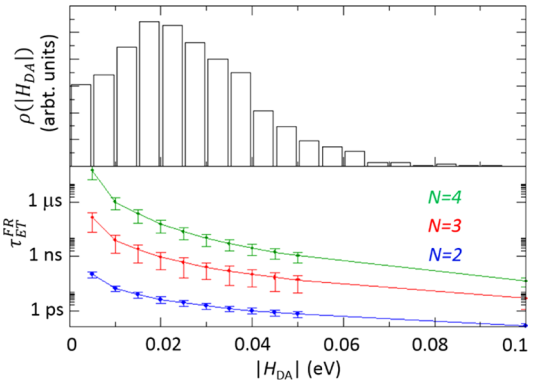

Figure 5. Sensitivity of the flickering resonance ET times to the electronic coupling in *Xl*(6−4)PL. (Top) Histogram of $|H_{DA}|$ from MD simulations. (Bottom) Vertical bars represent the standard deviation of values obtained from the 26 sets of MD simulations (i.e., the variations of FR times with initial conditions).

DISCUSSION AND CONCLUSION

Charge migration along chains of amino-acid residues is arousing an ever increasing interest over the last years, since several proteins have been discovered, the biological functions of which may partially or even largely rely on such phenomenon.[37,95] Among them are the MauG/Methylamine Dehydrogenase complex of the *Paracoccus denitrificans* respiratory chain,[39] the ribonucleotide reductases,[96] and the family of DNA photolyases and cryptochromes.[1,2,37] Gray and Winkler also recently emitted a hypothesis that such phenomena may underlie basic mechanisms used by certain enzymes to prevent them from self-damage.[97] Indeed, metalloenzymes can involve highly oxidative intermediates to activate otherwise inert chemical bonds (e.g., aliphatic C−H bonds). In situations of weak coupling between oxidative intermediates production and substrate oxidation, the oxidative power of the transient intermediates may turn against the protein instead of attacking the substrate. Protein damage would decrease enzyme efficiency. Gray and Winkler suggested that evolution has favored the emergence of electron escaping routes in proteins to shuttle electrons away from the active sites, for example, when no substrates are present. Being shifted to the enzymes surfaces, electron holes would then be reduced by cellular reductants. Chains of tryptophan and tyrosine residues have been proposed to serve as such electron escape routes.[35,98]

The molecular mechanisms, by which the structure and dynamics of proteins control the speed and directionality of multiple step charge migration involving amino-acid residues, are still largely unknown. Charge migration in proteins belonging to the CRYs and PLs family represents an interesting natural system to learn more about these processes. In this article, we investigated electron/hole transfer in a protein of the family that involves a chain of four redox-active tryptophan residues instead of the "traditional" tryptophan triad. Müller et al. recently showed by transient absorption spectroscopy measurements that Trp_{370} (the fourth residue of the chain) has a strong impact on photoreduction in *Xl*(6−4)PL[17] but could not say with absolute certainty that this residue is really the terminal electron donor. Alternatively, it could only stabilize the charge on Trp_{319}^{o+}, the third tryptophan of the chain (note that Trp_{319}^{o+} and Trp_{370}^{o+} cation radicals are chemically the same species and cannot therefore be easily distinguished by transient absorption spectroscopy). The calculations reported here indicate a downhill nature of charge migration along the tetrad. Individual intertryptophan ET rates have not been resolved so far in *Xl*(6−4)PL. The sampling rate used in ref 17 sets an upper value of time resolution to 50 ns, but based on the analogy with pump−probe experiments performed on related proteins, we expect the individual ET rates to take place in the picosecond time scale.[41,92] Here we analyzed charge migration through two different mechanisms: incoherent hopping under the framework of Marcus theory and coherent tunneling via the recently proposed flickering resonance mechanism.

In the framework of Marcus theory, the activation free energy is determined by relative values of ΔG° and λ. ΔG° is typically of minus a few tenths of electronvolts in CRYs and PLs; λ should thus not be too large ($\gtrsim$ 1 eV) to allow picosecond ET.

DOI: 10.1021/jacs.5b10938
J. Am. Chem. Soc. 2016, 138, 1904−1915

Previous nanosecond MD simulations of *E. coli* PL led to very large values of λ (1.6−2.6 eV) that were incompatible with picosecond ET[25,26] (note also that contrary to the present work, induction was not self-consistently taken into account in past studies). Following previous works of picosecond charge migration in the PRC,[32] we investigated the influence of protein relaxation length on the computed Δg_o and λ_o^{St}. For a given pair of trajectories, the values of these quantities exhibit large fluctuations with the simulation length, and we noted significant deviations between reorganization energies calculated from the Stokes shift and from the variance of the energy gap fluctuations. This is reminiscent of the conclusions drawn by Matyushov and co-workers on the PRC.[32,33,58] On the other hand, we found that averaging over multiple initial protein configurations largely damps these fluctuations, and effective Marcus theory parameters could be determined within energy windows of a few hundredths of electronvolts on the time scale covered by the ET process. Given these results for *Xl*(6−4)PL charge migration, it would be interesting to reinvestigate more deeply the influence of initial conditions on charge migration in the PRC.

It is certainly important to discuss the differences that exist between the simulation protocol used in this study and the one developed by Matyushov and collaborators (see, for example, ref 99 for a recent review). In order to deal with nonergodic effects due to the high rate of electron transfer, we studied the effect of sampling length on the calculation of ET characteristic times. Intuitively, the relevant sampling length τ_{samp} to be chosen is the one that leads to an ET characteristic time $\tau_{MT} \approx \tau_{samp}$. Limiting the sampling length to this value prevents to sample motions taking place on longer time scales. Moreover, we used multiple initial conditions to deal with the unknown initial state of the system. On the other hand, Matyushov and collaborators use the concept of dynamically restrained ensembles[99] in which the phase space accessible to the system is restricted to dynamical modes whose frequencies are higher than the ET process. In practice, ET constants (reorganization energies, rate constants, ...) are determined iteratively and self-consistently from integration of data extracted from long equilibrium MD simulations over sliding windows, the length of which is imposed by the ET characteristic time. Both methods are thus not exactly identical but are expected to give qualitatively similar results.

We addressed the issue of nonequilibrium for ET within the tryptophan tetrad by allowing each transient state (CT2 or CT3) to relax only during 25 ps between two electron transfers (see Scheme 1). This protocol is empirical and guided by experimental estimations of ET rates. It is justified a posteriori in our case because the computed ET characteristic times are close to 25 ps. Such protocol cannot be easily generalized when one has no clue about the ET rate. In the work of Matyushov and collaborators, nonequilibrium effects in the PRC are dealt with by applying a nonergodicity scaling factor to the reaction free energy computed from long equilibrium MD simulations.[33]

The presence of a four-tryptophan chain opens the possibility for a resonant tunneling mechanism over more than two sites. This eventuality was tested via the flickering resonance model of Zhang et al.[43,44] In their original article, these authors used the model to reinterpret experimental and computation data of hole transfer in DNA hairpins. Their conclusion was that transport via the FR should be possible over 3−4 bases. They also showed that exponential D−A distance dependence of ET rate is not necessarily a signature of superexchange and may be confused with FR. In DNA hairpins, FR is competitive with tunneling thanks to relatively large coupling between sites (0.1 eV) compared to typical energy gap fluctuations. Blumberger tested the FR model for ET in multiheme proteins.[45] It was concluded that FR could hardly be competitive with hopping as a consequence of the small electronic coupling (2 meV) between heme sites. Our results on *Xl*(6−4)PL suggest that FR may compete with hopping depending on the initial state of the proteins but only for three-tryptophan chains. The proximity of site energy levels and of rather sufficiently large electronic coupling (25 meV on average) permits substantial probabilities to reach multi-resonant states through tunneling. Importantly, FR rates were found to be very sensitive to the initial conditions of the MD simulations and to the electronic coupling values. Overall, the picture that emerges from our study is a possible mixture of incoherent hopping and multistate tunneling channels, though the former is likely to be dominant. The configuration of the protein at the moment of photoexcitation determines the intertryptophan electronic coupling strength and the relative positions of the energy levels, in turn favoring (or not) the occurrence of each channel that eventually can be superposed. Our results should motivate future research aimed at probing the relevance of the FR in CRYs and PLs. On the theoretical and computational level, more sophisticated FR models are needed to make more accurate predictions. We proposed a mixed quantum-classical formulation of the FR to treat the inner-sphere contributions at the quantum level. This development has been done in the spirit of past developments of the Marcus theory.[52−54] We think eq 8 should be useful to investigate flickering resonance for ET processes taking place in the inverted regime. It will also be necessary to better characterize the transition from multistate tunneling to hopping with nuclear relaxation. Indeed, nuclear relaxation of tryptophan, tyrosine, or methionine side chains is expected to take place within a few femtoseconds,[100] a process that should damp coherent oscillations and so the transport time. These aspects are probably not accurately described with the available models. On the experimental side, because different reactive channels are likely to be mixed, it will probably be difficult to assess their relative contributions. To this end, it has been suggested to take advantage of the distinct temperature dependences of the hopping and flickering resonance channels.[44,101] Site-directed mutagenesis of CRYs and PLs that target neighboring amino-acid residues of the tetrad may also bring valuable information if these mutations affect the energy site fluctuations (supposing their relative positions remain unchanged).

Together with the experimental results reported in ref 17, the present work has established the implication of the fourth tryptophan of the tetrad in *Xl*(6−4)PL as the final electron donor in FAD photoreduction. It is likely that a similar conclusion applies to other members of the CRY/PL family containing this Trp tetrad.[15] Regarding the possible involvement of cryptochromes in magnetoreception, the present study suggests that, given the current scarcity of high-quality samples of animal CRYs, animal (6−4)PLs are much better models for studies of CRY-associated magnetosensitivity than the previously investigated *Arabidopsis thaliana* CRY or bacterial CPD PL, which not only lack the fourth tryptophan but also the photoexcitation of which gives rise to radical pairs with lifetimes that deviate from those generated in animal CRYs by several orders of magnitude.[10,24,102,103]

DOI: 10.1021/jacs.5b10938
J. Am. Chem. Soc. 2016, 138, 1904−1915

■ ASSOCIATED CONTENT

Supporting Information

The Supporting Information is available free of charge on the ACS Publications website at DOI: 10.1021/jacs.5b10938.

Simulation data not shown in the main text: RMSD of protein backbone atoms; ET thermodynamics parameters for steps 2 and 3; sensitivity of H_{DA} to relative positions of tryptophan residues; displacement of normal modes of tryptophan residues upon oxidation; validation of the QM+MM approach for ET in CRYs and PLs; calculation details of statistical uncertainties (PDF)

■ AUTHOR INFORMATION

Corresponding Authors

*pavel.muller@cea.fr

*aurelien.de-la-lande@u-psud.fr

Notes

The authors declare no competing financial interest.

■ ACKNOWLEDGMENTS

We are grateful to Klaus Brettel for illuminating discussions. We acknowledge the WESTGRID (Canada) network for providing us with substantial computational resources. This work was performed using HPC resources from GENCI [CCRT/CINES/IDRIS] (Grant 2014-2015, project number x2015076913). P.M. acknowledges the support of the French Agence Nationale de Recherche (ANR, Grant ANR-12-BSV8-0001). This work was supported by the ANR program Investissements d'Avenir du LabEx PALM (Grant ANR-10-LABX-0039-PALM).

■ REFERENCES

(1) Sancar, A. *Chem. Rev.* **2003**, *103*, 2203−2238.

(2) Chaves, I.; Pokorny, R.; Byrdin, M.; Hoang, N.; Ritz, T.; Brettel, K.; Essen, L.-O.; van der Horst, G. T. J.; Batschauer, A.; Ahmad, M. *Annu. Rev. Plant Biol.* **2011**, *62*, 335−364.

(3) Wang, J.; Du, X.; Pan, W.; Wang, X.; Wu, W. *J. Photochem. Photobiol., C* **2015**, *22*, 84−102.

(4) Ritz, T.; Adem, S.; Schulten, K. *Biophys. J.* **2000**, *78*, 707−718.

(5) Kondoh, M.; Shiraishi, C.; Müller, P.; Ahmad, M.; Hitomi, K.; Getzoff, E. D.; Terazima, M. *J. Mol. Biol.* **2011**, *413*, 128−137.

(6) Müller, P.; Bouly, J.-P. *FEBS Lett.* **2015**, *589*, 189−192.

(7) Yang, H.-Q.; Wu, Y.-J.; Tang, R.-H.; Liu, D.; Liu, Y.; Cashmore, A. R. *Cell* **2000**, *103*, 815−827.

(8) Mouritsen, H. In *Sturkie's Avian Physiology*, 6th ed.; Scanes, C. G., Ed.; Academic Press: San Diego, 2015; pp 113−133.

(9) Liedvogel, M.; Mouritsen, H. *J. R. Soc., Interface* **2010**, *7*, S147−S162.

(10) Solov'yov, I. A.; Chandler, D. E.; Schulten, K. *Biophys. J.* **2007**, *92*, 2711−2726.

(11) Nießner, C.; Denzau, S.; Gross, J. C.; Peichl, L.; Bischof, H.-J.; Fleissner, G.; Wiltschko, W.; Wiltschko, R. *PLoS One* **2011**, *6*, e20091.

(12) Lee, A. A.; Lau, J. C. S.; Hogben, H. J.; Biskup, T.; Kattnig, D. R.; Hore, P. J. *J. R. Soc., Interface* **2014**, *11*, 20131063.

(13) Henbest, K. B.; Maeda, K.; Hore, P. J.; Joshi, M.; Bacher, A.; Bittl, R.; Weber, S.; Timmel, C. R.; Schleicher, E. *Proc. Natl. Acad. Sci. U. S. A.* **2008**, *105*, 14395−14399.

(14) Maeda, K.; Henbest, K. B.; Cintolesi, F.; Kuprov, I.; Rodgers, C. T.; Liddell, P. A.; Gust, D.; Timmel, C. R.; Hore, P. J. *Nature* **2008**, *453*, 387−390.

(15) Müller, P.; Ahmad, M. *J. Biol. Chem.* **2011**, *286*, 21033−21040.

(16) Maeda, K.; Robinson, A. J.; Henbest, K. B.; Hogben, H. J.; Biskup, T.; Ahmad, M.; Schleicher, E.; Weber, S.; Timmel, C. R.; Hore, P. J. *Proc. Natl. Acad. Sci. U. S. A.* **2012**, *109*, 4774−4779.

(17) Müller, P.; Yamamoto, J.; Martin, R.; Iwai, S.; Brettel, K. *Chem. Commun.* **2015**, *51*, 15502−15505.

(18) Aubert, C.; Vos, M. H.; Mathis, P.; Eker, A. P. M.; Brettel, K. *Nature* **2000**, *405*, 586−590.

(19) Lee, E.; Medvedev, E. S.; Stuchebrukhov, A. A. *J. Phys. Chem. B* **2000**, *104*, 6894−6902.

(20) Prytkova, T. R.; Beratan, D. N.; Skourtis, S. S. *Proc. Natl. Acad. Sci. U. S. A.* **2007**, *104*, 802−807.

(21) Cheung, M. S.; Daizadeh, I.; Stuchebrukhov, A. A.; Heelis, P. F. *Biophys. J.* **1999**, *76*, 1241−1249.

(22) Cailliez, F.; Müller, P.; Gallois, M.; de la Lande, A. *J. Am. Chem. Soc.* **2014**, *136*, 12974−12986.

(23) Solov'yov, I. A.; Domratcheva, T.; Schulten, K. *Sci. Rep.* **2014**, *4*, 3845.

(24) Hong, G.; Pachter, R. *J. Phys. Chem. B* **2015**, *119*, 3883−3892.

(25) Krapf, S.; Koslowski, T.; Steinbrecher, T. *Phys. Chem. Chem. Phys.* **2010**, *12*, 9516−9525.

(26) Woiczikowski, P. B.; Steinbrecher, T.; Kubař, T.; Elstner, M. *J. Phys. Chem. B* **2011**, *115*, 9846−9863.

(27) Lüdemann, G.; Woiczikowski, P. B.; Kubař, T.; Elstner, M.; Steinbrecher, T. B. *J. Phys. Chem. B* **2013**, *117*, 10769−10778.

(28) Lüdemann, G.; Solov'yov, I. A.; Kubař, T.; Elstner, M. *J. Am. Chem. Soc.* **2015**, *137*, 1147−1156.

(29) Marcus, R. A.; Sutin, N. *Biochim. Biophys. Acta, Rev. Bioenerg.* **1985**, *811*, 265−322.

(30) King, G.; Warshel, A. *J. Chem. Phys.* **1990**, *93*, 8682−8692.

(31) Warshel, A.; Parson, W. W. *Annu. Rev. Phys. Chem.* **1991**, *42*, 279−309.

(32) LeBard, D. N.; Kapko, V.; Matyushov, D. V. *J. Phys. Chem. B* **2008**, *112*, 10322−10342.

(33) LeBard, D. N.; Matyushov, D. V. *J. Phys. Chem. B* **2009**, *113*, 12424−12437.

(34) LeBard, D. N.; Martin, D. R.; Lin, S.; Woodbury, N. W.; Matyushov, D. V. *Chem. Sci.* **2013**, *4*, 4127−4136.

(35) Gray, H. B.; Winkler, J. R. *Proc. Natl. Acad. Sci. U. S. A.* **2015**, *112*, 10920−10925.

(36) Shih, C.; Museth, A. K.; Abrahamsson, M.; Blanco-Rodriguez, A. M.; Di Bilio, A. J.; Sudhamsu, J.; Crane, B. R.; Ronayne, K. L.; Towrie, M.; Vlček, A.; Richards, J. H.; Winkler, J. R.; Gray, H. B. *Science* **2008**, *320*, 1760−1762.

(37) Warren, J. J.; Ener, M. E.; Vlček, A., Jr; Winkler, J. R.; Gray, H. B. *Coord. Chem. Rev.* **2012**, *256*, 2478−2487.

(38) Takematsu, K.; Williamson, H.; Blanco-Rodríguez, A. M.; Sokolová, L.; Nikolovski, P.; Kaiser, J. T.; Towrie, M.; Clark, I. P.; Vlček, A.; Winkler, J. R.; Gray, H. B. *J. Am. Chem. Soc.* **2013**, *135*, 15515−15525.

(39) Tarboush, N. A.; Jensen, L. M. R.; Yukl, E. T.; Geng, J.; Liu, A.; Wilmot, C. M.; Davidson, V. L. *Proc. Natl. Acad. Sci. U. S. A.* **2011**, *108*, 16956−16961.

(40) Geng, J.; Dornevil, K.; Davidson, V. L.; Liu, A. *Proc. Natl. Acad. Sci. U. S. A.* **2013**, *110*, 9639−9644.

(41) Lukacs, A.; Eker, A. P. M.; Byrdin, M.; Brettel, K.; Vos, M. H. *J. Am. Chem. Soc.* **2008**, *130*, 14394−14395.

(42) Lauz, M.; Eckhardt, S.; Fromm, K. M.; Giese, B. *Phys. Chem. Chem. Phys.* **2012**, *14*, 13785−13788.

(43) Zhang, Y.; Liu, C.; Balaeff, A.; Skourtis, S. S.; Beratan, D. N. *Proc. Natl. Acad. Sci. U. S. A.* **2014**, *111*, 10049−10054.

(44) Beratan, D. N.; Liu, C.; Migliore, A.; Polizzi, N. F.; Skourtis, S. S.; Zhang, P.; Zhang, Y. *Acc. Chem. Res.* **2015**, *48*, 474−481.

(45) Blumberger, J. *Chem. Rev.* **2015**, *115*, 11191−11238.

(46) Humphrey, W.; Dalke, A.; Schulten, K. *J. Mol. Graphics* **1996**, *14*, 33−38.

(47) Blumberger, J. *Phys. Chem. Chem. Phys.* **2008**, *10*, 5651−5667.

(48) de la Lande, A.; Gillet, N.; Chen, S.; Salahub, D. R. *Arch. Biochem. Biophys.* **2015**, *582*, 28−41.

(49) Kubař, T.; Elstner, M. *J. R. Soc., Interface* **2013**, *10*, 20130415.

(50) Kubař, T.; Elstner, M. *Phys. Chem. Chem. Phys.* **2013**, *15*, 5794−5813.

DOI: 10.1021/jacs.5b10938
J. Am. Chem. Soc. 2016, 138, 1904−1915

(51) Parson, W. W.; Chu, Z. T.; Warshel, A. *Biophys. J.* **1998**, *74*, 182−191.
(52) Kestner, N. R.; Logan, J.; Jortner, J. *J. Phys. Chem.* **1974**, *78*, 2148−2166.
(53) Efrima, S.; Bixon, M. *Chem. Phys.* **1976**, *13*, 447−460.
(54) Jortner, J.; Bixon, M. *J. Chem. Phys.* **1988**, *88*, 167−170.
(55) Marcus, R. A.; Siders, P. *J. Phys. Chem.* **1982**, *86*, 622−630.
(56) Onuchic, J. N. *J. Chem. Phys.* **1987**, *86*, 3925−3943.
(57) Warshel, A. *J. Phys. Chem.* **1982**, *86*, 2218−2224.
(58) Matyushov, D. V. *J. Chem. Phys.* **2013**, *139*, 025102.
(59) Matyushov, D. V. *Acc. Chem. Res.* **2007**, *40*, 294−301.
(60) Hopfield, J. J. *Proc. Natl. Acad. Sci. U. S. A.* **1974**, *71*, 3640−3644.
(61) Borrelli, R.; Capobianco, A.; Peluso, A. *Can. J. Chem.* **2013**, *91*, 495−504.
(62) Borrelli, R.; Peluso, A. *J. Chem. Phys.* **2003**, *119*, 8437−8448.
(63) Koster, A. M.; Calaminici, P.; Casida, M. E.; Dominguez, V. D.; Flores-Moreno, R.; Geudtner, G.; Goursot, A.; Heine, T.; Ipatov, A.; Janetzko, F.; del Campo, J. M.; Reveles, J. U.; Vela, A.; B, Z.; Salahub, D. R. *deMon2k program*; The deMon developers: Mexico City, 2011.
(64) Becke, A. D. *J. Chem. Phys.* **1993**, *98*, 5648−5652.
(65) Krishnan, R.; Binkley, J. S.; Seeger, R.; Pople, J. A. *J. Chem. Phys.* **1980**, *72*, 650−654.
(66) Borrelli, R.; Di Donato, M.; Peluso, A. *Theor. Chem. Acc.* **2007**, *117*, 957−967.
(67) Borrelli, R.; Di Donato, M.; Peluso, A. *J. Chem. Theory Comput.* **2007**, *3*, 673−680.
(68) Duschinski, F. *Acta Phisicochim URSS* **1937**, *7*, 551−556.
(69) Hu, L.; Farrokhnia, M.; Heimdal, J.; Shleev, S.; Rulíšek, L.; Ryde, U. *J. Phys. Chem. B* **2011**, *115*, 13111−13126.
(70) Wang, Z.-X.; Zhang, W.; Wu, C.; Lei, H.; Cieplak, P.; Duan, Y. *J. Comput. Chem.* **2006**, *27*, 781−790.
(71) Caldwell, J. W.; Kollman, P. A. *J. Phys. Chem.* **1995**, *99*, 6208−6219.
(72) Tipmanee, V.; Oberhofer, H.; Park, M.; Kim, K. S.; Blumberger, J. *J. Am. Chem. Soc.* **2010**, *132*, 17032−17040.
(73) Oberhofer, H.; Blumberger, J. *Angew. Chem., Int. Ed.* **2010**, *49*, 3631−3634.
(74) Case, D. A.; Darden, T. A.; Cheatham, I. T.E. ; Simmerling, C. L.; Wang, J.; Duke, R. E.; Luo, R.; Crowley, M.; Walker, R. C.; Zhang, W.; Merz, K. M.; Wang, B.; Hayik, S.; Roitberg, A.; Seabra, G.; Kolossváry, I.; Wong, K. F.; Paesani, F.; Vanicek, J.; Wu, X.; Brozell, S. R.; Steinbrecher, T.; Gohlke, H.; Yang, L.; Tan, C.; Mongan, J.; Hornak, V.; Cui, G.; Mathews, D. H.; Seetin, M. G.; Sagui, C.; Babin, V.; Kollman, P. A. *Amber 10*; University of California: San Francisco, 2008.
(75) Bordoli, L.; Kiefer, F.; Arnold, K.; Benkert, P.; Battey, J.; Schwede, T. *Nat. Protoc.* **2008**, *4*, 1−13.
(76) Tanida, H.; Tahara, E.; Mochizuki, M.; Yamane, Y.; Ryoji, M. *FEBS J.* **2005**, *272*, 6098−6108.
(77) Maul, M. J.; Barends, T. R. M.; Glas, A. F.; Cryle, M. J.; Domratcheva, T.; Schneider, S.; Schlichting, I.; Carell, T. *Angew. Chem., Int. Ed.* **2008**, *47*, 10076−10080.
(78) Dolinsky, T. J.; Nielsen, J. E.; McCammon, J. A.; Baker, N. A. *Nucleic Acids Res.* **2004**, *32*, W665−W667.
(79) Wu, Q.; Van Voorhis, T. *Phys. Rev. A: At., Mol., Opt. Phys.* **2005**, *72*, 024502.
(80) de la Lande, A.; Salahub, D. R. *J. Mol. Struct.: THEOCHEM* **2010**, *943*, 115−120.
(81) Řezáč, J.; Lévy, B.; Demachy, I.; de la Lande, A. *J. Chem. Theory Comput.* **2012**, *8*, 418−427.
(82) Calaminici, P.; Janetzko, F.; Köster, A. M.; Mejia-Olvera, R.; Zuniga-Gutierrez, B. *J. Chem. Phys.* **2007**, *126*, 044108.
(83) Kubas, A.; Hoffmann, F.; Heck, A.; Oberhofer, H.; Elstner, M.; Blumberger, J. *J. Chem. Phys.* **2014**, *140*, 104105.
(84) Kubas, A.; Gajdos, F.; Heck, A.; Oberhofer, H.; Elstner, M.; Blumberger, J. *Phys. Chem. Chem. Phys.* **2015**, *17*, 14342−14354.
(85) Adamo, C.; Barone, V. *J. Chem. Phys.* **1999**, *110*, 6158−6170.
(86) Mejía-Rodríguez, D.; Köster, A. M. *J. Chem. Phys.* **2014**, *141*, 124114.
(87) Hirshfeld, F. L. *Theoret. Chim. Acta* **1977**, *44*, 129−138.
(88) Wu, Q.; Van Voorhis, T. *J. Chem. Phys.* **2006**, *125*, 164105.
(89) R Development Core Team. R: A Language and Environment for Statistical Computing.; R Foundation for Statistical Computing: Vienna, Austria; 2012.http://www.R-project.org/.
(90) Plummer, M.; Best, N.; Cowles, K.; Vines, K. *R News* **2006**, *6*, 7−11.
(91) Kao, Y.-T.; Saxena, C.; He, T.-F.; Guo, L.; Wang, L.; Sancar, A.; Zhong, D. *J. Am. Chem. Soc.* **2008**, *130*, 13132−13139.
(92) Immeln, D.; Weigel, A.; Kottke, T.; Pérez Lustres, J. L. *J. Am. Chem. Soc.* **2012**, *134*, 12536−12546.
(93) Shirdel, J.; Zirak, P.; Penzkofer, A.; Breitkreuz, H.; Wolf, E. *Chem. Phys.* **2008**, *352*, 35−47.
(94) Brazard, J.; Usman, A.; Lacombat, F.; Ley, C.; Martin, M. M.; Plaza, P.; Mony, L.; Heijde, M.; Zabulon, G.; Bowler, C. *J. Am. Chem. Soc.* **2010**, *132*, 4935−4945.
(95) Giese, B.; Graber, M.; Cordes, M. *Curr. Opin. Chem. Biol.* **2008**, *12*, 755−759.
(96) Minnihan, E. C.; Nocera, D. G.; Stubbe, J. *Acc. Chem. Res.* **2013**, *46*, 2524−2535.
(97) Winkler, J. R.; Gray, H. B. *Philos. Trans. R. Soc., A* **2015**, *373*, 20140178.
(98) Polizzi, N. F.; Migliore, A.; Therien, M. J.; Beratan, D. N. *Proc. Natl. Acad. Sci. U. S. A.* **2015**, *112*, 10821−10822.
(99) Matyushov, D. V. *J. Phys.: Condens. Matter* **2015**, *27*, 473001.
(100) Narth, C.; Gillet, N.; Cailliez, F.; Lévy, B.; de la Lande, A. *Acc. Chem. Res.* **2015**, *48*, 1090−1097.
(101) Blumberger, J. Manuscript in preparation, 2015.
(102) Paulus, B.; Bajzath, C.; Melin, F.; Heidinger, L.; Kromm, V.; Herkersdorf, C.; Benz, U.; Mann, L.; Stehle, P.; Hellwig, P.; Weber, S.; Schleicher, E. *FEBS J.* **2015**, *282*, 3175−3189.
(103) Liedvogel, M.; Maeda, K.; Henbest, K.; Schleicher, E.; Simon, T.; Timmel, C. R.; Hore, P. J.; Mouritsen, H. *PLoS One* **2007**, *2*, e1106.

DOI: 10.1021/jacs.5b10938
J. Am. Chem. Soc. 2016, 138, 1904−1915